Integral Equation Modeling of Waveguide-Fed Planar Antennas

Ivica Stevanović[1,2], Francesco Merli[2], Pedro Crespo-Valero[3], Winfried Simon[4],
Sybille Holzwarth[4], Michael Mattes[2], and Juan R. Mosig[2]

[1]ABB Corporate Research
Segelhofstrasse 1K, CH-5405 Baden 5 Dättwil, Switzerland
Tel: +41 58 586 7103; Fax: +41 58 586 7312; E-mail: ivica.stevanovic@ch.abb.com, ivica.stevanovic@epfl.ch

[2]Laboratory of Electromagnetics and Acoustics, Ecole Polytechnique Fédérale de Lausanne (EPFL)
CH-1015 Lausanne, Switzerland
Tel: +41 21 693 4642, 5681, 4628; Fax: +41 21 693 2673
E-mail: francesco.merli@epfl.ch; michael.mattes@epfl.ch; juan.mosig@epfl.ch

[3]Schmid & Partner Engineering AG
Zeughausstrasse 43, CH-8004 Zurich, Switzerland
Tel: +41 44 245 9700; Fax: +41 44 245 9779; E-mail: crespo@speag.ch

[4]IMST GmbH, Carl-Friedrich-Gauss Str. 2, D-47475 Kamp-Lintfort, Germany
Tel: +49 2842 981 247; Fax: +49 2842 981 499; E-mail: simon@imst.de; holzwarth@imst.de

_____

Abstract

This paper presents a method for the analysis of planar multilayered waveguide-fed antennas. The method combines mixed-potential integral equations (for laterally open regions) and modal-field integral equations (for laterally closed regions) with a seamless transition between the two domains. The method has been implemented in a numerical tool, and the simulation results of two waveguide-fed planar structures are presented. The results are in good agreement with both measurements and simulations obtained with other commercial electromagnetic tools. Comparisons in terms of memory utilization and simulation time have also been performed.

Keywords: Integral equations; moment methods; Green functions; waveguide antennas; microstrip arrays; microstrip antennas

1. Introduction

Nowadays, there exist a number of general electromagnetic tools (see [1-5] to mention only a few) able to analyze complex three-dimensional (3D) structures, including non-homogeneous materials or nonlinear elements. These methods rely on intensive computational effort, and require volume discretization of the whole geometry under analysis. They also require the introduction of an absorbing boundary around the discretized volume to emulate the radiation condition. All of this leads to large memory utilization and very long simulation times. These drawbacks are partially obviated by ever-advancing computer technology. Indeed, the rapid growth in processor speed and available memory, and the introduction of multi-core processor architectures and acceleration cards, have opened new, wide horizons for these general-purpose codes.

This being said, highly specialized computational EM tools can also take advantage of these technological improvements, and are inherently more accurate when applied within their natural limits. Hence, developing specifically tailored techniques, perfectly adapted to a narrow family of problems, will always remain a winning strategy. This is the gist of this paper.

One such class of problems is waveguide-fed planar antennas. This type of antenna is now receiving a lot of attention as a good candidate for low-loss, high-rate wireless connections at frequencies between 20 and 100 GHz [6, 7]. Automotive applications are yet another interesting domain for these antennas. Intelligent cruise control and collision-avoidance radar require highly directional antenna arrays [8, 9]. These antennas need to be low cost, and need to satisfy strict size constraints dictated by automotive manufacturers. Waveguide-fed planar antenna arrays are advantageously used in these applications, thanks to their low profile and suitability for low-cost mass production. Realizing the feeding network in waveguide technology and the radiating structure in planar technology further reduces the feed losses, and enhances gain for a given radiating-aperture area.

Modeling and simulation of waveguide-fed planar antennas can be done using general techniques, such as Finite-Difference Time-Domain methods [8, 10], Finite-Element Methods [9, 11-14], or Finite-Integration Techniques [15, 16]. Hybrid finite-element/integral-equation techniques [17-19] can also be used where the Finite-Element Method is applied to modeling laterally bounded (waveguide) structures, and the integral-equation technique is used for laterally open (antenna) structures. However, this is a typical case where a more-specific approach – such as an integral-equation formulation solved using the Method-of-Moments (IE-MoM) – still remains the most suitable strategy. IE-MoM techniques are particularly well suited for the so-called 2.5D geometries, where the use of brute force and a huge number of unknowns can be replaced by a pre-processing analytical effort leading to the formulation of the pertinent Green's functions. Moreover, IE-MoM is well suited to modeling realistic excitations. It can produce results for scattering parameters and related near- and far-field quantities that are in general more accurate that those obtained with the general-purpose tools.

The mixed-potential integral-equation formulation [20] has been successfully applied in the analysis of planar antennas (open multilayered problems). The modal integral-equation formulation is an efficient method used in solving closed problems, such as multilayered waveguides or cavities [21]. Therefore, a well-balanced combination of these two integral-equation formulations, as proposed in this paper, should provide an excellent tool for analyzing 2.5D hybrid (open/closed) geometries, such as those appearing in waveguide-fed planar antennas.

The combined formulation should inherently account for dielectrics, ground planes, and the radiation condition in laterally unbounded structures, while being able to model accurately mode-dominated phenomena in waveguides and cavities.

Waveguide-fed patch antennas were already analyzed with IE-MoM strategies in [22]. However, only the waveguide excitation was taken into account, with no dielectric layers or metallizations present in the waveguide. Similarly, cavity-backed antennas with dielectric layers in both the cavity and the open planar structure were analyzed in [23], but no waveguide-excitation was been accounted for. In this paper, we present an integral-equation technique for modeling waveguide-fed planar antennas having an arbitrary number of dielectrics and embedded metallizations in both laterally closed (cavity) and open (planar antenna) regions, with a seamless transition between the two regions. The method has the advantage of a consistent integral-equation approach, which produces well-conditioned matrices and yields highly accurate results.

The paper is organized as follows. First, we outline the integral-equation technique applied to planar dielectric layered structures that are either laterally unbounded or embedded within rectangular waveguides. We give details for efficient computation of Green's functions, and the construction of Method-of-Moments matrices, in both laterally open and closed regions. Finally, software based on this integral-equation approach has been used to simulate two practical examples of waveguide-fed planar antennas. We compare the results of our simulations with measurements and results from other tools, and we discuss memory utilization and computational efficiency issues.

2. Integral Equations with Method of Moments

Consider a hybrid structure, composed of rectangular waveguide sections that feed a multilayered planar antenna (Figure 1). The antenna structure can have arbitrarily shaped conductive patches and slots in ground planes between different dielectric layers. Any waveguide section can also be filled by stratified dielectrics, and can include conductive patches or slots of arbitrary shapes, localized in planes perpendicular to the propagation direction.

Every patch surface is modeled using electric surface currents, $\mathbf{J}_E$. At every interconnection of two different waveguides and on every slot, the surface Equivalence Principle is applied. Magnetic surface currents, $\mathbf{J}_H$, (on both sides of the interface) are introduced in such a way as to ensure the continuity of the tangential component of the total electric field, $\mathbf{E}$:

$$\mathbf{E}_{tan}^{+} = \mathbf{E}_{tan}^{-} \Leftrightarrow \mathbf{J}_H^{+} = -\mathbf{J}_H^{-}. \tag{1}$$

Note that for unification purposes that will become clear later, we prefer ($\mathbf{J}_E$, $\mathbf{J}_H$) to denote electric and magnetic currents, and not ($\mathbf{J}$, $\mathbf{M}$).

In this way, each slot decouples the original problem into two equivalent sub-problems, one above and one below the slot interface. Each sub-problem can be either laterally unbounded (open problem) or enclosed in a rectangular waveguide (closed problem).

There are two additional boundary conditions that need to be ensured, which will result in the integral-equation formulation of the problem. The continuity of the tangential magnetic field ($\mathbf{H}$) on the slots and at the interconnections between two different waveguides has to be satisfied:

$$\mathbf{H}_{tan}^{+} = \mathbf{H}_{tan}^{-}. \tag{2}$$

Considering all the patches to be made of perfectly conducting metallizations, the tangential electric field on them has to vanish:
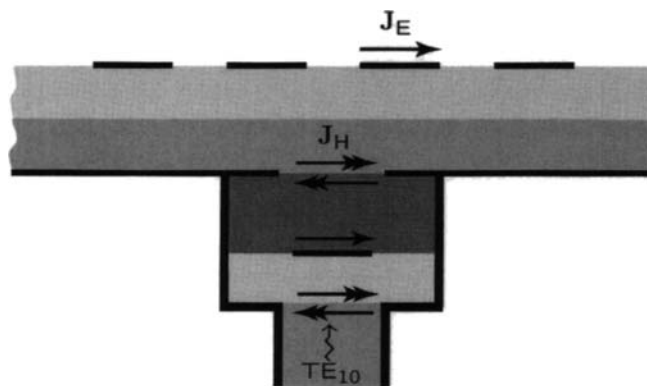

Figure 1. A general multilayered waveguide structure that feeds a multilayered antenna array.

$$E_{tan} = E_{tan}^{inc} + E_{tan}^{scatt} = 0, \qquad (3)$$

where E^{inc} and E^{scatt} are the incident and the scattered electric fields, respectively. For modeling lossy metalizations, the zero on the right-hand side of Equation (3) can be replaced by the Leontovich boundary condition [20].

Introducing field Green's functions (which correspond to the open or closed sub-problems), the scattered fields can be expressed as convolution integrals of the electric and/or magnetic sources and the corresponding Green's functions. The boundary conditions evolve this way into a system of integral equations with unknown electric and magnetic surface currents.

The Method of Moments technique is used for numerically solving the system of integral equations [24]. The unknown electric and magnetic currents are expanded into a set of basis functions. In order to model general shapes of magnetic and electric planar sources, sub-sectional (rectangular/triangular) basis functions have been selected, so the unknown sources can be expanded as follows:

$$J_Q(r') = \sum_k \alpha_{Qk} f_{Qk}(r'), \quad k = 1, \dots, N_Q, \qquad (4)$$

where the source index $Q = E$ represents a horizontal electric dipole (HED), and $Q = H$ represents a horizontal magnetic dipole (HMD). In the same expression, the α_{Qk} are the unknown coefficients in the expansion of the currents, and the f_{Qk} are the N_Q sub-sectional basis functions defined on electric ($Q = E$) or magnetic ($Q = H$) surfaces.

Using a Galerkin procedure, the basis functions serve also as test functions. In this way, the original coupled system of integral equations is transformed into an algebraic system of linear equations, with coefficients α_{Qk} as unknowns:

$$\begin{bmatrix} [R_{EE}] & [R_{EH}] \\ [R_{HE}] & [R_{HH}] \end{bmatrix} \begin{bmatrix} [\alpha_E] \\ [\alpha_H] \end{bmatrix} = \begin{bmatrix} [\gamma_E] \\ [\gamma_H] \end{bmatrix}. \qquad (5)$$

A Method-of-Moments element (k, l) in each submatrix can be written as

$$R_{PQ}(k, l) = \int_{S_k} f_{Pk}(r) dS \int_{S_l} \ddot{G}_{PQ}(r|r') f_{Ql}(r') dS'. \qquad (6)$$

The above is a compact notation, where both the observer index, P, and the source index, Q, can be either E (electric field, electric source) or H (magnetic field, magnetic source). $\ddot{G}_{PQ}$ stands for a specific multilayer Green's function. In the case where $R_{HH}(k, l)$ is an interaction between two basis functions defined on the same slot, it can be written as

$$R_{HH}(k, l) = \int_{S_k} f_{Hk}(r) dS \int_{S_l} \left[\ddot{G}_{HH}^+(r|r') + \ddot{G}_{HH}^-(r|r') \right] f_{Hl}(r') dS', \qquad (7)$$

where the superscripts "+" and "−" designate the magnetic-field Green's function for the sub-problem above and below the slot, respectively, connecting by this means the two otherwise uncoupled sub-problems.

3. Multilayered Green's Functions

As stated in the previous section, the study of sources embedded in a planar multilayered medium calls for the computation of the corresponding Green's function. This computation can be optimally performed by solving an equivalent transmission-line problem (Figure 2) [20, 25]. The source becomes a lumped generator, and every layer corresponds to a transmission-line section. The terminal impedance walls bounding the planar multilayered medium correspond to loading impedances. For instance, a semi-infinite terminal will be simulated by a matched load. Once the equivalent transmission-line problem is solved, the knowledge of voltages and currents at any z level allows a full solution of the original electromagnetic problem. In particular, voltages and currents at the connection points between transmission-line sections give the fields and the potentials at the interfaces of the layered medium.

Tables 1 and 2 summarize the expressions that relate spectral-domain field and potential Green's function components with voltages and currents in the equivalent transmission-line model. In these tables, k_z is the propagation constant in the z direction, and $k_\rho^2 = k_0^2 \mu_r \varepsilon_r - k_z^2 = k_x^2 + k_y^2$ is the transverse wavenumber. The characteristic impedances for the TE and TM modes are respectively given by

$$Z_c^{TE} = \frac{\omega \mu_0 \mu_r}{k_z}$$

and

$$Z_c^{TM} = \frac{k_z}{\omega \varepsilon_0 \varepsilon_r}.$$

These expressions are valid for both laterally open and closed multilayered structures. In the case of closed structures, k_ρ takes on discrete values corresponding to the cutoff wavenumbers of the associated waveguide. Note also that a transverse electric source
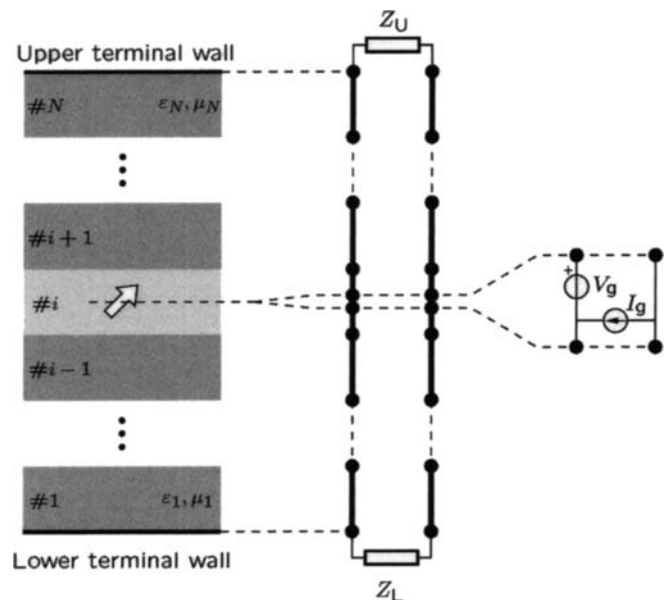

Figure 2. The equivalent transmission-line model of the Green's function problem [26].

Table 1. Analytical expressions of the field Green's function components in a multilayered medium in terms of currents and voltages in the equivalent transmission line model [23, 29].

Electric Source	
$\tilde{G}_{EJ}^{xx} = -\frac{1}{k_\rho^2}\left(k_y^2 V_{J_\rho}^{TE} + k_x^2 V_{J_\rho}^{TM}\right)$	$\tilde{G}_{HJ}^{xx} = -\frac{k_x k_y}{k_\rho^2}\left(I_{J_\rho}^{TE} - I_{J_\rho}^{TM}\right)$
$\tilde{G}_{EJ}^{yx} = \frac{k_x k_y}{k_\rho^2}\left(V_{J_\rho}^{TE} - V_{J_\rho}^{TM}\right)$	$\tilde{G}_{HJ}^{yx} = -\frac{1}{k_\rho^2}\left(k_y^2 I_{J_\rho}^{TE} + k_x^2 I_{J_\rho}^{TM}\right)$
$\tilde{G}_{EJ}^{xy} = \frac{k_x k_y}{k_\rho^2}\left(V_{J_\rho}^{TE} - V_{J_\rho}^{TM}\right)$	$\tilde{G}_{HJ}^{xy} = \frac{1}{k_\rho^2}\left(k_x^2 I_{J_\rho}^{TE} + k_y^2 I_{J_\rho}^{TM}\right)$
$\tilde{G}_{EJ}^{yy} = -\frac{1}{k_\rho^2}\left(k_x^2 V_{J_\rho}^{TE} + k_y^2 V_{J_\rho}^{TM}\right)$	$\tilde{G}_{HJ}^{yy} = \frac{k_x k_y}{k_\rho^2}\left(I_{J_\rho}^{TE} - I_{J_\rho}^{TM}\right)$

Magnetic Source	
$\tilde{G}_{EM}^{xx} = -\frac{k_x k_y}{k_\rho^2}\left(V_{M_\rho}^{TE} - V_{M_\rho}^{TM}\right)$	$\tilde{G}_{HM}^{xx} = -\frac{1}{k_\rho^2}\left(k_x^2 I_{M_\rho}^{TE} + k_y^2 I_{M_\rho}^{TM}\right)$
$\tilde{G}_{EM}^{yx} = \frac{1}{k_\rho^2}\left(k_x^2 V_{M_\rho}^{TE} + k_y^2 V_{M_\rho}^{TM}\right)$	$\tilde{G}_{HM}^{yx} = -\frac{k_x k_y}{k_\rho^2}\left(I_{M_\rho}^{TE} - I_{M_\rho}^{TM}\right)$
$\tilde{G}_{EM}^{xy} = -\frac{1}{k_\rho^2}\left(k_y^2 V_{M_\rho}^{TE} + k_x^2 V_{M_\rho}^{TM}\right)$	$\tilde{G}_{HM}^{xy} = -\frac{k_x k_y}{k_\rho^2}\left(I_{M_\rho}^{TE} - I_{M_\rho}^{TM}\right)$
$\tilde{G}_{EM}^{yy} = \frac{k_x k_y}{k_\rho^2}\left(V_{M_\rho}^{TE} - V_{M_\rho}^{TM}\right)$	$\tilde{G}_{HM}^{yy} = -\frac{1}{k_\rho^2}\left(k_y^2 I_{M_\rho}^{TE} + k_x^2 I_{M_\rho}^{TM}\right)$

Table 2. Analytical expressions for the potential Green's function components in a multilayered medium in terms of currents and voltages in the equivalent transmission-line model [23].

Electric Source	Magnetic Source
$\tilde{G}_A^{xx} = \frac{1}{j\omega} V_{J_\rho}^{TE}$	$\tilde{G}_F^{xx} = \frac{1}{j\omega} I_{M_\rho}^{TM}$
$\tilde{G}_A^{yy} = \frac{1}{j\omega} V_{J_\rho}^{TE}$	$\tilde{G}_F^{yy} = \frac{1}{j\omega} I_{M_\rho}^{TM}$
$\tilde{G}_V = -\frac{j\omega}{k_\rho^2}\left(V_{J_\rho}^{TE} - V_{J_\rho}^{TM}\right)$	$\tilde{G}_W = \frac{j\omega}{k_\rho^2}\left(I_{M_\rho}^{TE} - I_{M_\rho}^{TM}\right)$

J_ρ corresponds to a parallel current generator of $I_g = 1/(2\pi)$ for laterally unbounded and $I_g = 1$ for laterally bounded problems. A transverse magnetic source M_ρ corresponds to a series voltage generator with $V_g = 1/(2\pi)$ for laterally unbounded problems. $V_g = 1$ for laterally bounded problems.

The Sommerfeld choice for vector potentials reduces the full dyadic into only five nonzero components [27, 28]. Note that throughout this work, only planar electric and magnetic sources (at $z = $ constant) are considered.

3.1 Green's Function of Laterally Unbounded Multilayered Media

If a function, G, depends on transverse coordinates only through the radial source-observer distance $\rho = \sqrt{(x - x')^2 + (y - y')^2}$, then its spectral transform is only a function of the radial spectral coordinate $k_\rho = \sqrt{k_x^2 + k_y^2}$. We can then write the two-dimensional Fourier transform as a Hankel (Fourier-Bessel) transform, also called the Sommerfeld integral:

$$G(\rho,z,z') = S_n\{\tilde{G}(k_\rho,z,z')\} = \int_0^\infty J_n(k_\rho\rho)k_\rho^{n+1}\tilde{G}(k_\rho,z,z')\,dk_\rho,$$

$$(8)$$

where J_n is the Bessel function of the first kind of order n, and $\tilde{G}$ is a generic spectral Green's function depending on the variable $k_\rho = \sqrt{k_x^2 + k_y^2}$ and the vertical positions of the observer (z) and source (z') points. Thanks to the basic properties of the Bessel functions, only the Sommerfeld integrals of the order $n = 0$ and $n = 1$ are needed to find the potential and field Green's function components (Tables 1 and 2). The correspondence between the spectral and space domains for various expressions of $\tilde{G}$ can be summarized as in Table 3 (ϕ is the angle in cylindrical coordinates). The numerical evaluation of Sommerfeld integrals S_0 and S_1 can be efficiently performed using specially tailored algorithms [20, 30].

3.2 Efficient Evaluation of Method-of-Moments Matrix in Laterally Unbounded Sub-Problems

The interactions in the Method-of-Moments matrix corresponding to the laterally unbounded sub-problems can be computed differently, depending on the interfaces where source and observer rooftops are situated. If the source and the observer rooftops (basis and weight functions) belong to the same type of source (electric or magnetic), the potential Green's functions are used in order to obtain a milder singularity (R^{-1} for potentials, instead of R^{-3} for fields). This allows for the integrals to be computed numerically in two possible ways. In one strategy, the singularity can be extracted, treated analytically [31], and added to the remaining regular part, which can be computed using numerical integration. Another strategy is to solve the integral in polar coordinates, where the Jacobian of the transformation will cancel out the singularity, and the integral can be computed numerically [23, 32].

This means that in the final matrix of moments, every time that a convolution integral of the type $\ddot{G}_{EE} \otimes J_E$ appears in the

Table 3. The correspondence between the spectral- and space-domain Green's functions [29].

Spectral Domain	Space domain
$\tilde{G}$	$S_0\{\tilde{G}\}$
$jk_x\tilde{G}$	$-\cos\phi\, S_1\{\tilde{G}\}$
$jk_y\tilde{G}$	$-\sin\phi\, S_1\{\tilde{G}\}$
$jk_x jk_x\tilde{G}$	$\frac{\cos(2\phi)}{\rho} S_1\{\tilde{G}\} - \cos^2\phi\, S_0\{k_\rho^2\tilde{G}\}$
$jk_y jk_y\tilde{G}$	$-\frac{\cos(2\phi)}{\rho} S_1\{\tilde{G}\} - \sin^2\phi\, S_0\{k_\rho^2\tilde{G}\}$
$jk_x jk_y\tilde{G}$	$\frac{\sin(2\phi)}{\rho} S_1\{\tilde{G}\} - \frac{1}{2}\sin(2\phi) S_0\{k_\rho^2\tilde{G}\}$

integral equation, it will contribute to the corresponding Method-of-Moments matrix element with the term

$$R_{\mathrm{EE}}\left(k,l\right)=\left\langle \mathbf{f}_k,\bar{\mathbf{G}}_{\mathrm{EE}}\otimes\mathbf{f}_l\right\rangle \tag{9}$$

$$=-\mathrm{j}\omega\left\langle \mathbf{f}_k,\bar{\mathbf{G}}_A\otimes\mathbf{f}_l\right\rangle-\frac{1}{\mathrm{j}\omega}\left\langle \nabla\boldsymbol{\cdot}\mathbf{f}_k,G_V\otimes\left(\nabla\boldsymbol{\cdot}\mathbf{f}_l\right)\right\rangle,$$

where the inner product is defined as

$$\left\langle \mathbf{w}_k,\mathbf{h}_l\right\rangle=\int_{S_k}\mathbf{w}_k\boldsymbol{\cdot}\mathbf{h}_l\,\mathrm{d}S_k, \tag{10}$$

and the convolution integral is defined as

$$\bar{\mathbf{G}}_{\mathrm{EE}}\otimes\mathbf{f}_l=\int_{S_l}\bar{\mathbf{G}}_{\mathrm{EE}}\left(\mathbf{r}\middle|\mathbf{r}'\right)\mathbf{f}_l\left(\mathbf{r}'\right)\mathrm{d}S_l.$$

In the above equations, G_V is the scalar potential and $\bar{\mathbf{G}}_A$ represents the vector potential Green's function.

In the case of two rooftops belonging to different types of sources, field Green's functions are preferred (there is no singular interaction, since magnetic and electric currents are not supposed to share the same z level). The contribution to the corresponding Method-of-Moments matrix element is

$$R_{\mathrm{PQ}}\left(k,l\right)=\left\langle \mathbf{f}_k,\bar{\mathbf{G}}_{\mathrm{PQ}}\otimes\mathbf{f}_l\right\rangle, \tag{11}$$

for the case when $\mathbf{f}_k$ belongs to the electric source and $\mathbf{f}_l$ belongs to the magnetic source, or vice-versa.

In all cases, the numerical integration is done using cubature rules especially adapted to triangular or rectangular domains [33]. The Green's functions are also pre-computed and stored into two-dimensional tables at each frequency. The Green's function values needed to compute the numerical integrals are retrieved from the tables using efficient interpolation routines, which lead to very accurate results and much faster computation than if the Green's functions are evaluated directly.

3.3 Green's Function of Laterally Bounded Multilayered Media

Using the equivalent transmission-line networks to represent the waveguide sections, the field dyadic Green's functions are given by

$$\bar{\mathbf{G}}_{\mathrm{PQ}}\left(\mathbf{r}\mid\mathbf{r}'\right)=\sum_i\tilde{G}_{\mathrm{P}i}\left(z,z'\right)\mathbf{p}_i\left(x,y\right)\mathbf{q}_i\left(x',y'\right). \tag{12}$$

In the above compact notation, the vector mode functions $\mathbf{p}$ and $\mathbf{q}$ are the modal functions of either electric ($\mathbf{e}$) or of magnetic ($\mathbf{h}$) type. $\tilde{G}_{\mathrm{P}i}\left(z,z'\right)$ depends only on the observer index, P, and designates the associated spectral Green's function (from the equivalent transmission-line model) that corresponds to either the voltage ($\mathbf{p}=\mathbf{e}$) or the current ($\mathbf{p}=\mathbf{h}$). The index i represents the order number of the rectangular waveguide mode (TE$_{m,n}$, where

$m,n=0,1,2,...;mn\neq0$, or TM$_{m,n}$, where $m,n=1,2,3,...$). The expressions for the vector mode functions, $\mathbf{e}_i$ and $\mathbf{h}_i$, for rectangular cross sections can be found in [34]. Using rectangular-waveguide Green's functions, Equation (12), the Method-of-Moments elements of Equation (6) can be written as

$$R_{\mathrm{PQ}}\left(k,l\right)=\sum_i\tilde{G}_{\mathrm{P}i}C_{\mathrm{P}}\left(k,i\right)C_{\mathrm{Q}}\left(l,i\right), \tag{13}$$

where

$$C_{\mathrm{P}}\left(k,i\right)=\int_{S_k}\mathbf{f}_{\mathrm{P}k}\left(x,y\right)\mathbf{p}_i\left(x,y\right)\mathrm{d}x\mathrm{d}y. \tag{14}$$

It can be noticed from the above equations that all the Method-of-Moments matrix coefficients are functions of only two different overlapping integrals, in particular, the overlapping integrals of the $\mathbf{e}$ and $\mathbf{h}$ vector mode functions with the vector basis functions. These integrals can be computed analytically because they have rectangular and/or triangular sub-sectional basis functions [21, 23].

3.4 Efficient Evaluation of Method-of-Moments Matrix in Laterally Bounded Sub-Problems

The extraction of the quasi-static term of the spectral Green's functions is performed for the efficient evaluation of the series appearing in Equation (13) [34, 36-38]. The main implication of this technique is that the original series are separated into frequency-independent and frequency-dependent series. The frequency-independent series are evaluated only once for a given geometry. As for the frequency-dependent series, they are evaluated for each point in frequency, but due to the extraction of the quasi-static part, the convergence is considerably enhanced. As a result, an important saving in computational time for the analysis of multilayered-media waveguide structures over a wide range of frequencies is achieved [23, 29].

4. Modal Excitation

Let the excitation of the waveguide be a source that produces a single mode (denoted by the index i). The field transverse to the z direction can be expressed in terms of the incident power wave, a_i, as

$$\mathbf{H}^{\mathrm{inc}}=\frac{a_i}{\sqrt{Z_i}}\mathbf{h}_i, \tag{15}$$

where Z_i is the modal impedance and $\mathbf{h}_i$ is the magnetic-field vector modal function of the considered mode.

Let an aperture, A_1, be in the reference plane in which we compute the reflection coefficient. Let it be discretized into a number of sub-sectional (rectangular and/or triangular) basis functions, $\mathbf{f}_{\mathrm{H}k}$, for all indices $k=1,...,N_{\mathrm{H}}$ for which $S_k\subset A_1$. The excitation vector in the Method-of-Moments system of equations in Equation (5) can then be expressed as follows:

$$\gamma_{Hk} = -2 \int_{S_k} \mathbf{H}^{inc} \cdot \mathbf{f}_{Hk} \, dS, \qquad (16)$$

where the coefficient of two comes from the "mirrored" magnetic field [40].

After having solved the system, we obtain, among the others, the unknown coefficients α_{Hk}, used to expand the magnetic current on the aperture A_1 in a given set of basis functions. It can be shown that the reflection coefficient on the aperture A_1 can then be expressed as [39]

$$s_{11} = -1 - \frac{1}{a_i} \frac{1}{\sqrt{Z_i}} \sum_k \alpha_{Hk} \int_{S_k} \mathbf{f}_{Hk} \cdot \mathbf{h}_i \, dS. \qquad (17)$$

5. Numerical Examples

In this section, we analyze two waveguide-fed planar antennas using the numerical tool, based on the theory presented so far. We compare the solutions with measurements and with the results obtained with other simulation tools. No symmetry or mirror planes have been used in any of the simulations.

5.1 Waveguide-Fed Microstrip Patch Antenna

The geometry of the rectangular microstrip patch antenna in this example was taken from [22]. The patch was excited through a slot on the end wall of an empty rectangular WR90 waveguide, as shown in Figure 3. In our simulation, the planar patch and slot surfaces were discretized with 189 rectangular basis functions. The fundamental TE_{10} mode of the rectangular waveguide was used as excitation. The number of modes used to compute the Method-of-Moments matrix for the inside (waveguide) structure was 5000 for the static sum and 1000 for the dynamic sum, which led to a maximum memory utilization of 7 MB. The VSWR and the reflec-

Figure 3. The geometry of a rectangular microstrip patch antenna (taken from [22]). The dimensions were $l_w = 22.86$ mm, $w_w = 10.16$ mm, $l_a = 14$ mm, $w_a = 0.3$ mm, $l_p = 14$ mm, $w_p = 11.7$ mm. The patch was printed on a substrate with $\varepsilon_r = 2.2$, $\tan\delta = 0.001$, and thickness $h = z_2 - z_1 = 3.15$ mm.
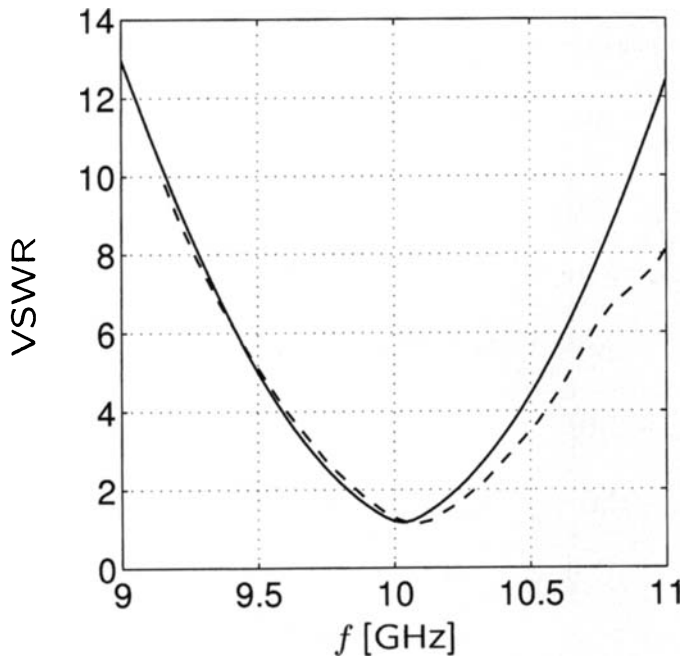
Figure 4. The VSWR of the waveguide-excited rectangular patch antenna: our results (solid lines) and measured values taken from [22] (dashed lines).

tion-coefficient phase of the antenna are shown in Figure 4 and Figure 5, respectively. The solid lines represent the simulation results, and the dashed lines represent the measured values taken from [22]. Good agreement with the measurements can be observed.

The same structure was simulated using the FEM-based frequency-domain solver Ansoft *High Frequency Structure Simulator*© (*HFSS*) [1] and the Finite-Integration Technique- (FIT-) based frequency-domain solver CST *Microwave Studio*© (*MWS*) [2]. The reflection coefficients computed using these different tools agreed well with our simulations, and are shown in Figure 6.

When comparing memory utilization and simulation time, the following considerations must be taken into account. Our solver accounts for dielectrics and ground planes as laterally unbounded structures. It asks only for the discretization of surface (metallization) sources; the dielectric layers, ground planes, and radiation conditions are inherently present in the Green's functions used. Therefore, this approach is well suited for the analysis of these types of 2.5D geometries. On the other hand, general solvers based on the FEM and FIT ask for volume discretization and the introduction of an air box around the radiating structure, with absorbing boundary conditions on the box's surface to emulate the radiation condition. This leads to larger memory utilization and somewhat longer simulation times, but allows for more-generic complex structures with non-homogeneous dielectrics to be analyzed.

In the *HFSS* simulations, a rectangular air box with the absorbing boundary conditions on its surface was placed far enough from the radiating structure of the antenna ($\sim \lambda/4$, with λ being the wavelength at the lowest simulation frequency) to ensure accurate results. The following simulation parameters were used: a maximum of 16 passes with a target convergence of 0.01, an adaptive frequency of 11 GHz, and 20% of maximum refinement per pass with a minimum of two converged passes. This led to 12599 tetrahedra to achieve the convergence, and a corresponding maximum memory utilization of 118 MB.
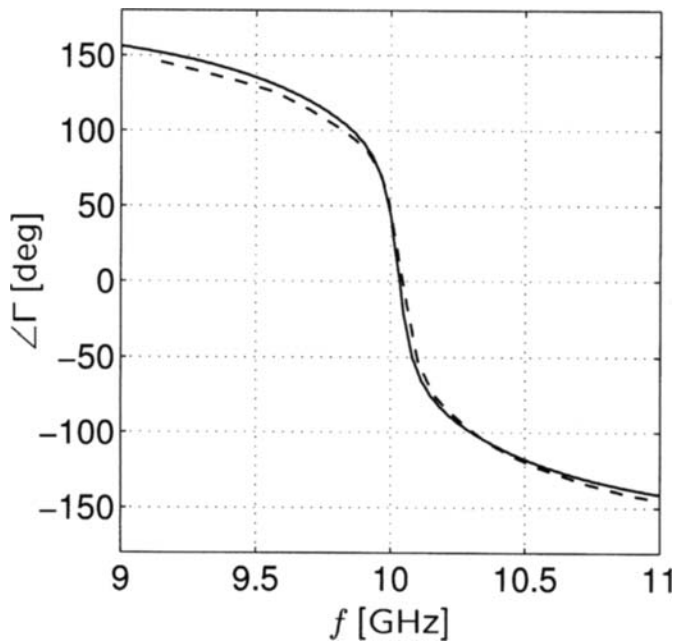
Figure 5. The phase of the reflection coefficient for the waveguide-excited rectangular patch antenna: our results (solid lines) and measured values taken from [22] (dashed lines).
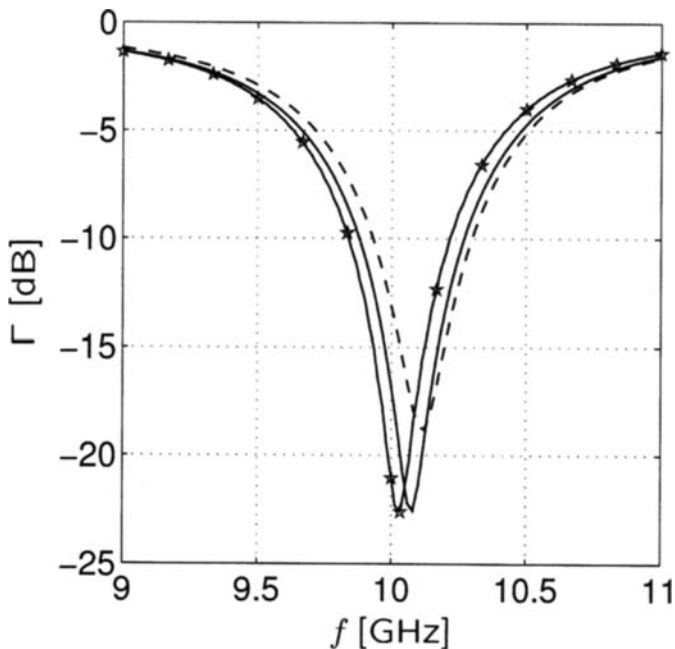

Figure 6. The reflection coefficient of the waveguide-excited rectangular patch antenna obtained using different simulation tools: our results (solid line with asterisks), *HFSS* (solid line), and CST *MWS* (dashed line).

In CST *MWS*, we used exactly the same geometry (including the air box dimensions) and the simulation parameters as in the *HFSS* simulations. The discretization that achieved accurate results led to 118262 tetrahedra, which corresponded to a peak memory utilization of 1.05 GB.

All the simulations were run on the same PC (Pentium 4 processor at 3.2 GHz with 3 GB of RAM). On this machine, our

solver took 2 minutes 51 seconds for the whole simulation (with 101 equally distributed frequency points in the range 9-11 GHz, and 2 seconds for the frequency-independent part of the procedure). This led to 1.7 seconds per frequency point. The *HFSS* simulation took 15 minutes 46 seconds (with 101 frequency points and 1 minute 18 seconds for adaptive mesh), for an average of 8.5 seconds per frequency point. Concerning the frequency-domain simulation with CST *MWS*, the setup took 29 minutes 45 seconds for the whole simulation (with five interpolation points and 22 minutes for the adaptive mesh), for an average of 92 seconds per frequency.

5.2 Waveguide-Fed Planar Antenna Array

The geometrical layout of our second example, a waveguide-fed planar antenna array, is shown in Figures 7-9. This antenna was part of a radar module operating at 24.125 GHz. It had a waveguide-to-stripline transition, optimized in such a way that the radiation of the transition did not disturb the radiation pattern of the patch array. This was achieved by a special patch/slot combination [8].

A snapshot of the mesh used in our simulation tool, which had 3070 basis functions (unknowns), is shown in Figure 8. The fundamental TE_{10} mode of the rectangular waveguide was used as excitation. The number of modes used to compute the Method-of-Moments matrix for the inside (waveguide) structure was 5000 for the static sum and 1000 for the dynamic sum.

The input parameters of the antenna were computed at the waveguide port, and the reflection coefficient is shown in Figure 10. The line with symbols represents the simulated values, and the dashed line represents measurements. The simulation was per-
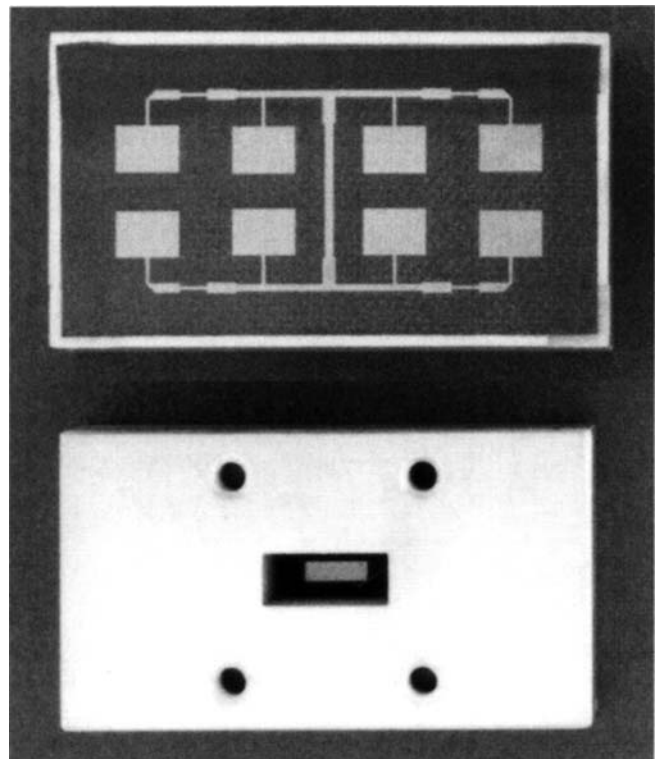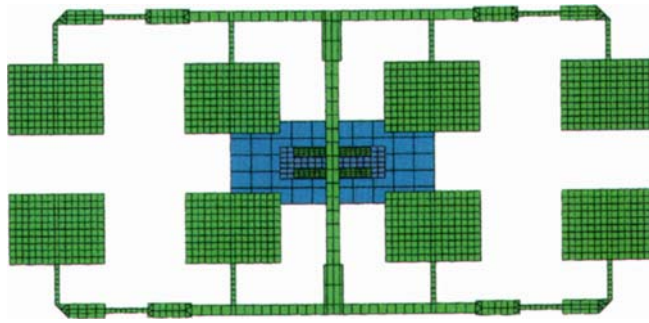

Figure 7. A waveguide-fed patch array.

Figure 8. The layout of the discretized geometry used to simulate the waveguide-fed patch array using our solver. The patch array was printed on a Capton dielectric layer ($\varepsilon_r = 2.2$, $h = 0.787$ mm) and placed on top of the waveguide. The two rectangular waveguide irises and a patch were printed on the opposite sides of another Capton layer, situated within the waveguide. The blue rectangle on the bottom represents the WR42 waveguide's cross section ($a = 10.7$ mm, $b = 4.3$ mm).
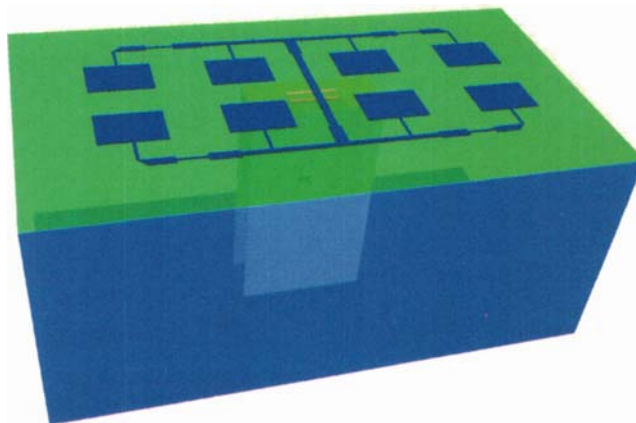

Figure 9. The three-dimensional geometry of the waveguide-fed patch array (from the *EMPIRE* graphical user interface).

formed on a PC with an Intel Core 2 Duo CPU T8300 at 2.4 GHz and with 3 GB of RAM. The whole simulation, with 61 discrete frequency points, took 73 minutes, or 73 seconds per frequency point, with a maximum memory utilization of 176 MB.

The same structure was simulated using the FDTD-based simulation tool $EMPIRE^{TM}$ [4], and the results are shown in the same figure with the gray line. The $EMPIRE$ simulations were performed on a Dell Precision 7400 with two Xeon 5472 CPUs at 3 GHz. The simulation took 100 seconds, and a maximum memory utilization of 317 MB. It should be pointed out that $EMPIRE$ is an extremely speed-optimized tool. For each simulation geometry and each processor architecture, it automatically creates specially suited assembler code. Furthermore, this assembler code is capable of using all the available multiple cores in the computer.
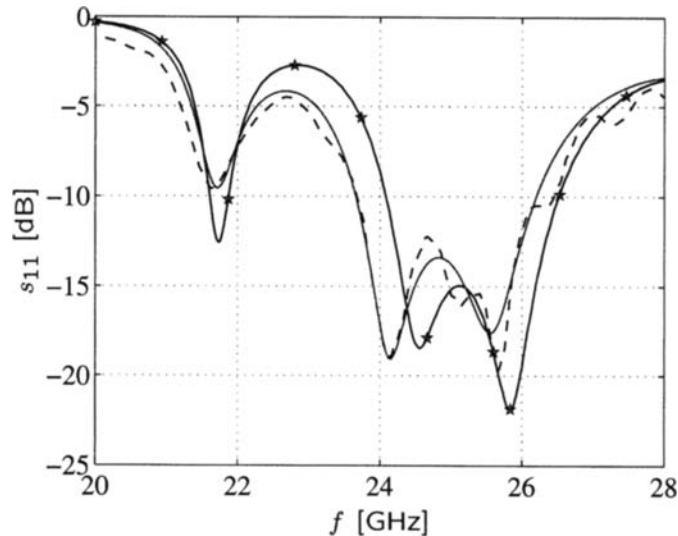
Figure 10. The reflection coefficient of the waveguide-fed patch array. Shown are results obtained using the theory presented (solid line with asterisks), the measured reference results (dashed line) [8], and the results obtained using $EMPIRE$ (gray line).
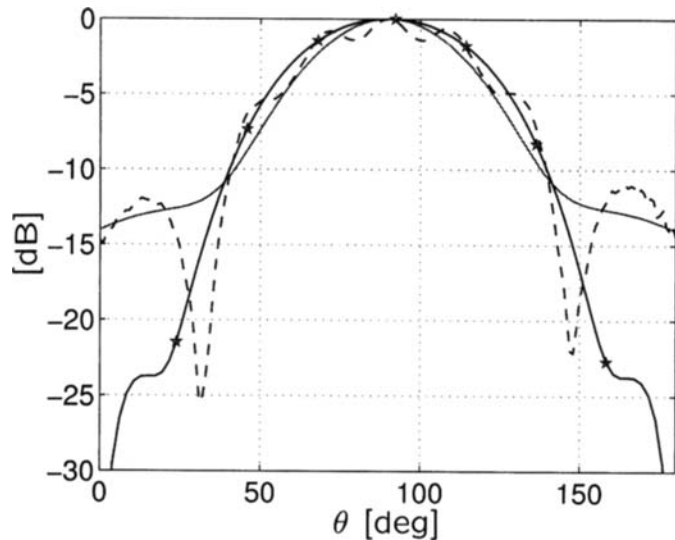

Figure 11. The co-polar radiation pattern in the E plane: computed using our method (solid line with asterisks), measurements (dashed line), and simulations using $EMPIRE$ (gray line).
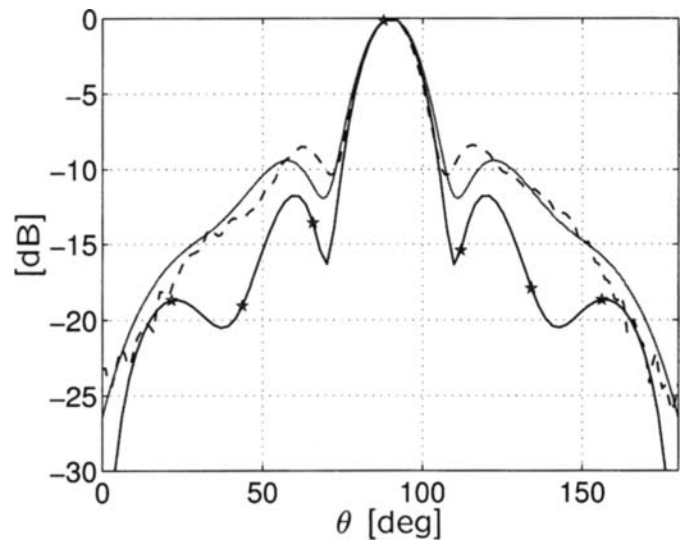

Figure 12. The co-polar radiation pattern in the H plane: computed using our method (solid line with asterisks), measurements (dashed line), and simulations using $EMPIRE$ (gray line).

Finally, we computed and measured the radiation pattern of the patch array at $f = 24.125$ GHz. The results are shown in Figures 11 and 12. It is worth noting that in our simulations, the ground plane with the slots between the waveguide and the antenna was considered to be infinitely large, and therefore the radiation pattern is shown only in the broadside direction.

6. Conclusion

In this paper, we have presented an integral-equation analysis of multilayered waveguide-fed antennas and arrays. The method combines mixed-potential integral equations for laterally open regions with modal-field integral equations for laterally closed regions, using a seamless transition between the two. An electromagnetic solver based on this approach was developed. The results of simulations of two waveguide-fed planar antennas were presented. These results were in good agreement with both measurements and the simulations obtained using other commercial electromagnetic tools. Comparisons in terms of memory utilization and simulation time were also performed. They showed that our integral-equation algorithm is very competitive when compared to sophisticated general electromagnetic tools.

7. Acknowledgments

8. References

1. Ansoft High Frequency Structure Simulator v11.1, http://www.ansoft.com/products/hf/hfss/, viewed on May 25, 2009.

2. CST Microwave Studio (Educational License), http://www.cst.com/Content/Products/MWS/Overview.aspx, viewed on May 25, 2009.

3. SEMCAD-X, http://www.semcad.com/simulation/, viewed on May 25, 2009.

4. EMPIRE XCcell, http://www.empire.de/, viewed on May 25, 2009.

5. FEKO, http://www.feko.info, viewed on May 25, 2009.

6. M. Ondo and J. Hirokawa, "High-Gain and High-Efficiency Single-Layer Slotted Waveguide Arrays in 60 GHz Band," Tenth International Conference on Antennas and Propagation Digest, April 14-17, 1997, Edinburgh, UK, **1**, pp. 464-468.

7. M. Samardzija, T. Kai, J. Hirokawa, and M. Ondo, "Single-Layer Waveguide Feed for Uniform Plane TEM-Wave in Over-sized-Rectangular Waveguide with Hard-Surface Sidewalls," *IEEE Transactions on Antennas and Propagation*, **AP-54**, 10, October 2006, pp. 2813-2819.

8. S. Holzwarth, W. Simon, and D. Heberling, "Simulation and Realisation of a Waveguide-Fed Planar Antenna Array," Millennium Conference on Antennas & Propagation Digest, April 9-14, Davos, Switzerland, pp. 1-4.

9. F. Kolak and C. Eswarappa, "A Low Profile 77 GHz Three Beam Antenna for Automotive Radar," 2001 IEEE International Microwave Symposium Digest, May 20-25, 2001, Phoenix, AZ, **2**, pp. 1107-1110.

10. A. Taflove and S. C. Hagness, *Computational Electrodynamics: The Finite-Difference Time-Domain Method, Third Edition*, Norwood, MA, Artech House, 2005.

11. D. P. Gray and L. Shafai, "Numerical Study of Waveguide Endwall Slot Feed Microstrip Arrays," *Electronics Letters*, **37**, 11, May 2001, pp. 673-675.

12. P. Herrero and J. Schoebel, "A WR-6 Rectangular Waveguide to Microstrip Transition and Patch Antenna at 140 GHz Using Low-Cost Solutions," 2008 IEEE Radio and Wireless Symposium Digest, January 22-24, 2008, Orlando, FL, pp. 355-358.

13. R. Alkhatib and R. Marzolf, "Waveguide-Fed Directive Antennas Based on Focusing System for Millimeter-Wave Applications," *Microwave and Optical Technology Letters*, **48**, 8, 2006, pp. 1592-1594.

14. J. L. Volakis, A. Chatterjee, and L. C. Kempel, *Finite Element Method for Electromagnetics: Antennas, Microwave Circuits, and Scattering Applications*, New York, IEEE Press, 1998.

15. W. Wu, J. Yin and N. Yuan, "Design of an Efficient X-band Waveguide-Fed Microstrip Patch Array," *IEEE Transactions on Antennas and Propagation*, **AP- 55**, 7, July 2007, pp. 1933-1939.

16. M. Clemens and T. Weiland, "Discrete Electromagnetism with the Finite Integration Technique," *Progress in Electromagnetics Research*, **PIER 32**, 2001, pp. 65-87.

17. J. Jin and J. Volakis, "TM Scattering by an Inhomogeneously Filled Aperture in a Thick Conducting Plane," *IEE Proceedings, Part H – Microwaves, Antennas and Propagation*, **137**, 3, June 1990, pp. 153-159.

18. P. Haddad and D. Pozar, "Characterisation of Aperture Coupled Microstrip Patch Antenna with Thick Ground Plane," *Electronics Letters*, **30**, 14, July 1994, pp. 1106-1107.

19. J.-M Jin and J. L. Volakis, "A Hybrid Finite Element Method for Scattering and Radiation by Microstrip Patch Antennas and Arrays Residing in a Cavity," *IEEE Transactions on Antennas and Propagation*, **AP-39**, 11, November 1991, pp. 1598-1604.

20. J. R. Mosig, "Integral-Equation Technique," in T. Itoh (ed.), *Numerical Techniques for Microwave and Millimeter-Wave Passive Structures*, New York, Wiley, 1989, Chapter 3, pp. 133-213.

21. P. Crespo-Valero, I. Stevanović, D. Llorens del Río, and J. R. Mosig, "On the Coupling Integrals Arising in the Method of Moments Formulation of Laterally Bounded Structures," *IEEE Transactions on Microwave Theory and Techniques*, **56**, 12, December 2008, pp. 2885-2892.

22. M.-H. Ho, K. A. Michalski, and K. Chang, "Waveguide Excited Microstrip Patch Antenna – Theory and Experiment," *IEEE Transactions on Microwave Theory and Techniques*, **42**, 8, August 1994, pp. 1114-1125.

23. A. Álvarez-Melcón, *Application of the Integral Equation Technique to the Analysis and Synthesis of Multilayered Printed Shielded Microwave Circuits and Cavity Backed Antennas*, PhD dissertation, Ecole Polytechnique Fédérale de Lausanne, Switzerland, 1998, Thèse No. 1901.

24. R. Harrington, *Field Computation by Moment Methods, Second Edition*, New York, IEEE Press, 1993.

25. P. Crespo-Valero, *Electromagnetic Modelling of Planar Circuits in Bounded Layered Media*, PhD dissertation, Ecole Polytechnique Fédérale de Lausanne, Switzerland, 2007, Thèse No. 3746.

26. I. Stevanović, *Modeling Challenges in Computational Electromagnetics: Large Planar Multilayered Structures and Finite-Thickness Irises*, PhD dissertation, Ecole Polytechnique Fédérale de Lausanne, Switzerland, 2005, Thèse No. 3212.

27. K. A. Michalski and D. Zheng, "Electromagnetic Scattering and Radiation by Surfaces of Arbitrary Shape in Layered Media, Part I: Theory," *IEEE Transactions on Antennas and Propagation*, **AP-38**, 3, March 1990, pp. 335-344.

28. K. A. Michalski and D. Zheng, "Electromagnetic Scattering and Radiation by Surfaces of Arbitrary Shape in Layered Media, Part II: Implementation and Results for Contiguous Half-Spaces," *IEEE Transactions on Antennas and Propagation*, **AP-38**, 3, March 1990, pp. 345-352.

29. T. Grzegorczyk, *Integrated 3D Antennas for Millimeter-Wave Applications: Theoretical Study and Technological Realization*,

PhD dissertation, Ecole Polytechnique Fédérale de Lausanne, Switzerland, 2000, Thèse No. 2299.

30. J. R. Mosig and F. E. Gardiol, "Analytical and Numerical Techniques in the Green's Function Treatment of Microstrip Antennas and Scatterers," *IEE Proceedings, Part H – Microwaves, Optics and Antennas*, **130**, 2, March 1983, pp. 175-182.

31. D. R. Wilton, S. M. Rao, A. W. Glisson, D. H. Schaubert, O. M. Al-Bundak, and C. M. Butler, "Potential Integrals for Uniform and Linear Source Distributions on Polygonal and Polyhedral Domains," *IEEE Transactions on Antennas and Propagation*, **AP-32**, 3, March 1984, pp. 276-281.

32. N. Morita, N. Kumagai, and J. Mautz, *Integral Equation Methods for Electromagnetics*, Norwood, MA, Artech House, 1990.

33. R. Cools, Encyclopaedia of Cubature Formulas, http://www.cs.kuleuven.ac.be/~nines/research/ecf/ecf.html, viewed on May 25, 2009.

34. N. Marcuvitz, *Waveguide Handbook*, New York, McGraw-Hill, 1951.

35. L. Lewin, *Theory of Waveguides*, London, Butterworths, 1975.

36. C. J. Railton and S. A. Meade, "Fast Rigorous Analysis of Shielded Planar Filters," *IEEE Transactions on Microwave Theory and Techniques*, **40**, May 1992, pp. 978-985.

37. G. V. Eleftheriades, J. R. Mosig, and M. Guglielmi, "A Fast Integral Equation Technique for Shielded Planar Circuits Defined on Nonuniform Meshes," *IEEE Transactions on Microwave Theory and Techniques*, **44**, December 1996, pp. 2293-2296.

38. M. Mattes, *Contribution to the Electromagnetic Modelling and Simulation of Waveguide Networks Using Integral Equations and Adaptive Sampling*, PhD dissertation, Ecole Polytechnique Fédérale de Lausanne, Switzerland, 2003, Thèse No. 2693.

39. I. Stevanović, P. Crespo-Valero, and J. R. Mosig, "An Integral-Equation Technique for Solving Thick Irises in Rectangular Waveguides," *IEEE Transactions on Microwave Theory and Techniques*, **54**, 1, January 2006, pp. 189-197.
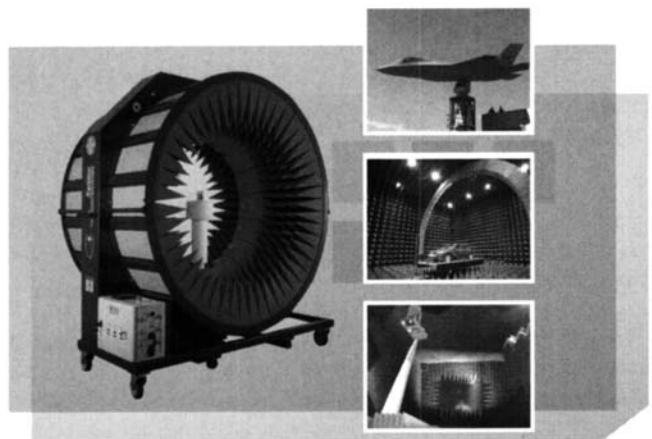
40. J. Van Bladel, *Electromagnetic Fields*, New York, McGraw-Hill, 1964.

41. http://www.antennasvce.org, viewed on May 25, 2009. ⊕